

An absolute test for axicon surfaces

Jun Ma,^{1,2,*} Christof Pruss,¹ Rihong Zhu,² Zhishan Gao,² Caojin Yuan,¹ and Wolfgang Osten¹

¹Institut für Technische Optik, Universität Stuttgart, Pfaffenwaldring 9, Stuttgart, 70569, Germany

²School of Electronic Engineering and Optoelectronic Techniques, Nanjing University of Science and Technology, Nanjing, 210094, China

*Corresponding author: optmj@yahoo.cn

Received March 15, 2011; revised April 22, 2011; accepted April 22, 2011;
posted April 25, 2011 (Doc. ID 144062); published May 25, 2011

We present a method for absolute testing of axicon surfaces in a null test setup. The absolute test exploits the symmetry of axicons, which allows us to introduce a shift of the surface under test in both the axial and rotational directions while still maintaining the null test condition. With two shifts of the surface under test and four measurements, the interferometer and null optics error can be removed. The absolute surface local deviation can be obtained by wavefront reconstruction with a double-side spiral-path direct integration method. A simulation of the method, including typical systematic as well as statistical errors as input, is presented to estimate the error propagation. Experimental absolute test results of a 90° axicon surface are given. © 2011 Optical Society of America

OCIS codes: 120.3180, 120.6650.

Axicon elements have been used in numerous applications due to their unique optical properties [1,2]. Therefore, investigations to improve their characterization are pursued with much attention [3–5]. The interferometric null test is one of the standard methods when high accuracy is required. Null testing of nonflat surfaces requires a null optic, such as a computer generated hologram (CGH), that adapts the plane wave of the interferometer to the surface under test. The obtained wavefront measurement contains contributions from the surface under test ϕ_{axicon} and from the interferometer error ϕ_{sys} , as well as unavoidable statistical errors ϕ_{noise} and misalignment errors ϕ_{mis} :

$$\Phi(\rho, \theta) = \phi_{\text{axicon}}(\rho, \theta) + \phi_{\text{sys}}(\rho, \theta) + \phi_{\text{noise}}(\rho, \theta) + \phi_{\text{mis}}(\rho, \theta). \quad (1)$$

In the following, we will skip for the sake of simplicity the statistical error, considering it later in the simulation and the choice of numerical methods. ϕ_{sys} contains errors introduced by the interferometer, such as errors of the reference surface or errors of the null lens. The separation of these errors from the measurement is required to obtain an absolute measurement result. Solutions have been reported based on CGH that reconstruct multiple wavefronts [6,7]. Recently, a novel method was proposed as a simple absolute test for flat surfaces [8]. The separation of test surface errors from interferometer errors is obtained by shifting the surface under test by small amounts in two orthogonal directions. The difference between the measurements gives a measure of the test surface's slope that can be integrated numerically to yield the absolute shape. In this contribution, we present the extension of this method to the absolute test of axicon surfaces. Shifting methods require that the surface under test can be shifted or rotated without losing the null test condition. Although axicon surfaces are highly aspheric, their linear generatrix allows this extension: it can be rotated and shifted along the optical axis.

The method requires four measurements in two independent groups (Fig. 1): two measurements with the test surface shifted axially by $\pm\Delta Z$ [Fig. 1(b)] and rotating it

by $\pm\Delta\theta$ [Fig. 1(c)]. Since only the surface under test is moved, the interferometer error ϕ_{sys} remains constant.

Equation (2) gives the measured wavefronts for the rotational direction shift $\pm\Delta\theta$:

$$\Phi^{\pm\Delta\theta}(\rho, \theta) = \phi_{\text{axicon}}(\rho, \theta \pm \Delta\theta) + \phi_{\text{sys}}(\rho, \theta). \quad (2)$$

For the axial translation ΔZ , Fig. 2 shows a specific characteristic of this null test configuration, here illustrated with a CGH as the null optics. The gradient singularity in the tip of the axicon leads to a ring-shaped interferogram and, correspondingly, to a ring-shaped CGH with inner and outer radius r_i and r_o . These dimensions depend on the distance Z_0 between the CGH and the vertex of the axicon, as well as the axicon geometry:

$$r_i = Z_0 \times \tan(\alpha/2), \quad (3)$$

$$r_o = 2 \times h \times \tan(\alpha/2) + r_i, \quad (4)$$

with the axicon cone angle α and height h . The width of the ring remains independent of Z_0 . If the vertex of the surface under test touches the CGH, the ring becomes a circle with diameter r_o .

The axial shift ΔZ translates into a radial shear with a constant shearing distance. The wavefronts we measure are given as

$$\Phi^{\pm\Delta z}(\rho, \theta) = \phi_{\text{axicon}}(\rho \pm \Delta Z \times \cot(\alpha/2), \theta) + \phi_{\text{sys}}(\rho, \theta). \quad (5)$$

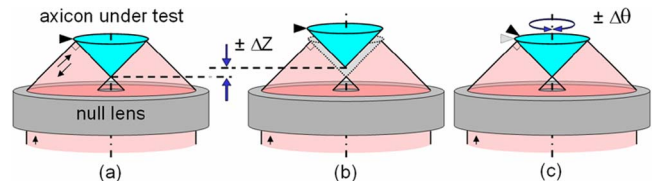


Fig. 1. (Color online) Shifting positions required for the absolute test. Test setup for testing an axicon in reflection with (a) a null lens, (b) axial translation, and (c) rotation.

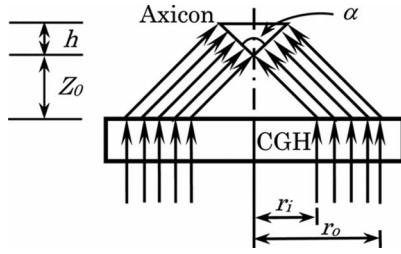


Fig. 2. Measurement configuration of CGH and axicon surface. Effective rays of CGH with r_i and r_o as the boundaries' radii.

In a stable setup, the system error stays the same for all four measurements. It is removed by using Eqs. (6) and (7), leading to wavefront differences in two orthogonal directions (rotational and radial):

$$\Phi^{\Delta\theta}(\rho, \theta) - \Phi^{-\Delta\theta}(\rho, \theta) = \phi(\rho, \theta + \Delta\theta) - \phi(\rho, \theta - \Delta\theta), \quad (6)$$

$$\Phi^{\Delta z}(\rho, \theta) - \Phi^{-\Delta z}(\rho, \theta) = \phi(\rho + \Delta\rho, \theta) - \phi(\rho - \Delta\rho, \theta). \quad (7)$$

In principle, only three measurements would be required to obtain the gradient in two directions. It has, however, been shown in practice that it is beneficial to take two separate pairs of measurements for each shifting direction, since then the stability requirement for the setup is minimal. It only needs to span the time between two subsequent measurements.

The choice of shifting distance influences the absolute surface reconstruction. It is a trade-off between information reconstruction in the frequency domain and suppression of error propagation (noise and misalignment). In order to simplify the surface reconstruction process, we project the obtained rotational and radial differences into differences in the X and Y directions, following the sampling directions of the camera. The transformation follows Eq. (8):

$$\begin{pmatrix} \Phi^{\Delta x} \\ \Phi^{\Delta y} \end{pmatrix} (x, y) = \begin{pmatrix} \Delta x & 0 \\ 0 & \Delta y \end{pmatrix} \cdot \begin{pmatrix} \cos\theta & -\sin\theta/\rho \\ \sin\theta & \cos\theta/\rho \end{pmatrix} \cdot \begin{pmatrix} \Phi^{\Delta z}/(2 \times \Delta\rho) \\ \Phi^{\Delta\theta}/(2 \times \Delta\theta) \end{pmatrix}. \quad (8)$$

Note that this projection requires a known center of rotation in camera pixel coordinates. An error will show as a twisted wavefront component after the subsequent integration. Since this kind of error is unlikely to occur in real optical surfaces, it can be utilized to detect an incorrect center of rotation.

If Δx and Δy are set to be 1 pixel, then the problem is changed to a standard problem in wavefront reconstruction. For this problem, many approaches have been published, e.g., iterative estimation algorithms for general shaped pupils [9,10], and a linear least squares method from annular Zernike polynomials for annular wavefronts [11]. However, these algorithms show problems at the boundaries of narrow annular wavefronts or are ineffective for larger array sizes of 200×200 pixels or

more. Direct integration methods, such as integration by many orbits (IMO [12]), have been shown to be robust in terms of error propagation. We developed a direct integration method adapted to the integration of annular areas, which we call spiral-path direct integration (SDI). A specific of SDI is that, for each point, we select two paths, clockwise and anticlockwise. This makes all points in the integration area have a similar average integration path, which is important in suppressing effects of error propagation.

Figure 3 illustrates the basic calculation method of SDI, with the two integration paths L and R from the common starting point s to a target point t . The paths follow Archimedes spiral lines and thus always remain inside the annulus area, avoiding the above-mentioned boundary problems. The two paths are averaged. This gives a similar integration length over the entire area, decreasing efficiently the nonuniformity of the reconstruction error in the tangential direction.

To estimate the performance of the method, we simulated the measurement of an imperfect sample in an imperfect setup and compared the result of the reconstruction with the known sample deviations. For our simulation, typical aberrations found in CGHs written in polar coordinates [13] are taken into account, as well as the alignment errors of the sample and white noise, to consider random errors, such as sensor noise of the interferogram registration. The simulated alignment errors include $\pm 1 \mu\text{m}$ of translation uncertainty and $\pm 15 \text{ arcsec}$ of rotation uncertainty. The aberrations from the CGH contain spoke-type errors from the fabrication of the CGH and an astigmatism contribution from a small amount of tilt that is introduced to prevent backreflections from the CGH substrate. A part of the astigmatism is motivated with electromagnetic effects that show when linearly polarized light from the interferometer interacts with the high line density (approximately 1117 line pairs/mm) rotationally symmetric grating structures. Figure 4(a) shows the total system error we have used for the simulation, while Fig. 4(b) shows the errors of the simulated surface under test, which we have chosen to be similar to the spoke-shaped error of the CGH, to test the capability of our method to separate the different error sources. Figure 4(c) shows the difference between the reconstructed surface under test and the known sample deviations we used for the simulation. Simulations with no noise and smaller shifting distances show that the small residual error of the reconstructed wavefront can be explained mainly by the added noise and derivatives approximations.

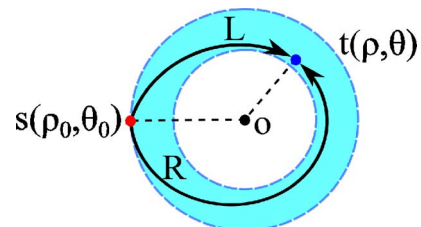


Fig. 3. (Color online) SDI diagram. Red point at left, starting point of the integration; blue point at upper right, target point of the integration.

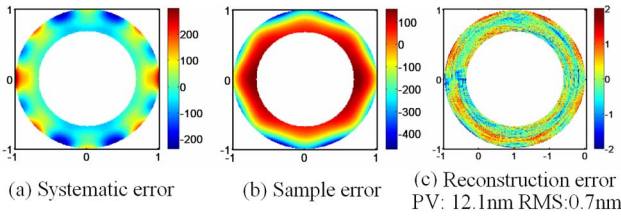


Fig. 4. (Color online) (a) Simulation of an absolute axicon measurement on a model interferometer with system error and (b) measuring a surface under test with errors, yielding the (c) reconstruction error.

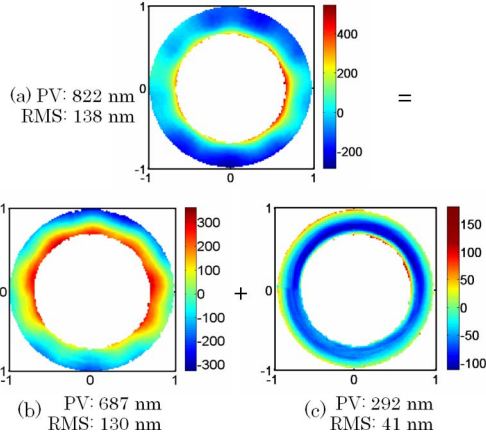


Fig. 5. (Color online) (a) Experimental result is split into the (b) systematic error and the (c) surface topography error.

To test the principle, we carried out the experiment with a commercial interferometer (FISBA μ Phase 2HR, PZT phase-shift, plane reference surface, mounted on a two-stage mechanical frame ALI 200 from Schneider Optikmaschinen). The collimated wavefront from the interferometer is transformed to an axicon wavefront with a high-line-density CGH [14], fabricated with scanning beam interference lithography, a special laser writing technique suitable for the efficient generation of high-resolution periodic structures. The CGH is a radial grating with a constant grating period of 894.943 nm, corresponding to a deflection angle of 45° required to test the axicon surface with a cone angle of 90° in a null test. To prevent substrate backreflections, the CGH is used under a small tilt angle. A linear alignment grating structure simplifies the correct tilt alignment.

The mechanical alignment of the axicon surface is realized by high-resolution micrometer calipers provided by the ALI 200 (axis translation) and an additional rotation air bearing (rotation about the symmetry axis). All axes are equipped with encoders ($1\ \mu\text{m}$ axis translation and $0.2\ \text{arc} \times \text{min}$ rotation). A fine alignment minimizing the difference between each pair of shifts in terms of tilt and coma ensured that the misalignment term ϕ_{mis} remained constant between the measurements and, therefore, it is subtracted in the evaluation procedure. Figure 5 depicts the measurement results, showing that the measurement [Fig. 5(a)] contains a considerable amount of systematic interferometer error [Fig. 5(b)]. The absolute test reveals that the non-rotationally symmetric errors

seen in the individual measurements are not caused by the surface under test but can be almost entirely attributed to the measurement setup. The surface under test shows almost perfect rotational symmetry [Fig. 5(c)].

In conclusion, we presented a method for the absolute test of axicon surfaces. The basic idea follows the simple measurement procedure proposed for plane surfaces [8], where accuracies of better than $\lambda/100$ peak to valley are expected for well-controlled conditions. Shifting the surface under test in the axial direction and rotating it by a small amount allows us to subtract the system error. Together with SDI, a novel wavefront reconstruction algorithm for narrow annular interferograms, this testing method provides a simple and robust method to obtain the axicon surface in an absolute manner. In our experiments, we achieved a repeatability of better than 2 nm rms with an instrument short-term repeatability of about 1 nm rms.

Leaving the simple geometry of plane surfaces adds some issues. Because of the integration involved, it is not possible to obtain the cone angle of the axicon surface in an absolute way. We have addressed this problem recently elsewhere [14]. Also, as for all interferometric measurements, the unavoidable misalignment of the surface introduces wavefront terms that are typically subtracted numerically and hence cannot be detected, such as tilt and coma.

The work presented in this Letter has been financed in part by the Baden-Württemberg Stiftung, and the National Natural Science Foundation of China (NSFC, Grants 60907002, 60977008). We thank Dr. J. Nam for the useful discussion on IMO and Dr. B. Heitkamp from Kugler GmbH, Germany, for providing the high-precision axicon samples.

References

1. V. Belyi, A. Forbes, N. Kazak, N. Khilo, and P. Ropot, *Opt. Express* **18**, 1966 (2010).
2. O. Brzobohatý, T. Cizmár, and P. Zemánek, *Opt. Express* **16**, 12688 (2008).
3. J. Hayes, K. L. Underwood, J. S. Loomis, R. E. Parks, and J. C. Wyant, *Appl. Opt.* **20**, 235 (1981).
4. M. Deangelis, S. Nicola, P. Ferraro, A. Finizio, and G. Pierattini, *Opt. Lasers Eng.* **39**, 155 (2003).
5. D. Kupka, P. Schlup, and R. A. Bartels, *Appl. Opt.* **47**, 1200 (2008).
6. S. Reichelt and H. J. Tiziani, *Opt. Commun.* **220**, 23 (2003).
7. K. Mantel, E. Geist, I. Harder, N. Lindlein, and G. Leuchs, *Opt. Lett.* **34**, 3178 (2009).
8. E. E. Bloemhof, *Opt. Lett.* **35**, 2346 (2010).
9. F. Roddier and C. Roddier, *Appl. Opt.* **30**, 1325 (1991).
10. W. Zou and J. P. Rolland, *J. Opt. Soc. Am. A* **22**, 938 (2005).
11. P. Hariharan, B. F. Oreb, and W. Zhou, *J. Mod. Opt.* **33**, 251 (1986).
12. J. Nam and J. Rubinstein, *J. Opt. Soc. Am. A* **25**, 1697 (2008).
13. S. Reichelt, M. Daffner, H. J. Tiziani, and R. Freimann, *J. Mod. Opt.* **49**, 1069 (2002).
14. J. Ma, C. Pruss, M. Häfner, B. Heitkamp, R. Zhu, Z. Gao, C. Yuan, and W. Osten, "Systematic analysis of the measurement of cone angles using high line density computer-generated holograms," *Opt. Eng.* (to be published).